■ Self-Assembly

Two-Dimensional Crystals from Reduced Symmetry Analogues of Trimesic Acid

Rachel A. Barnard, Ananya Dutta, Jennifer K. Schnobrich, Christine N. Morrison, Seokhoon Ahn, and Adam J. Matzger*[a]

Abstract: The two-dimensional assembly of multicarboxylated arenes is explored at the liquid–graphite interface using scanning tunneling microscopy. Symmetry variations were introduced via phenylene spacer addition and the influence of these perturbations on the formation of hydrogen-bonded motifs from an alkanoic acid solvent is observed. This work demonstrates the importance of symmetry in 2D crystal formation and draws possible links of this behavior to prediction of coordination modes in three-dimensional coordination polymers.

Introduction

Long-range order in a layer of molecules assembled on a substrate can result in a two-dimensional (2D) crystal. In such 2D crystals, favorable molecule–molecule and molecule–substrate interactions can be incorporated at the stage of molecular design to promote long-range order during self-assembly.[1] The number and type of available inter- and intramolecular interactions influence the pattern of the 2D crystal. As is the case in bulk crystallization, there is a drive towards close packing in monolayers to maximize intermolecular interactions. However, molecules that engage in directionally defined interactions are ideal for the formation of precisely ordered porous structures, and if the interactions are sufficiently strong these molecules are capable of overcoming close packed alternatives.

Trimesic acid (1,3,5-benzenetricarboxylic acid, **TMA**) is an archetypal, rigid, highly symmetric molecule offering three hydrogen-bonding moieties directionally favorable for the formation of ordered, nanoscale porous networks. The 2D self-assembly of **TMA** has been extensively studied in the literature at the solution/highly ordered pyrolytic graphite (HOPG) interface by STM.[2] This study focuses on 2D crystals formed from analogues of **TMA** where molecular symmetry is reduced within the series by the addition of one or more phenylene spacers (Figure 1). This strategy for reducing molecular symmetry is expected to reduce the symmetry of the resultant 2D crystal due to the loss of two- and/or threefold symmetry within the series; the approach has met with success in 3D crystal engineering of coordination polymers where the resul-

tant reduction of network symmetry thwarts interpenetration.[3] Therefore, the manifestation of symmetry reduction in controlling 2D assembly is of particular interest as a complexity-generating operation. During the structural investigation of various assemblies of the reduced symmetry analogues of **TMA**, six different phases were observed including four different plane groups and a disordered assembly. Similarities in the segregation of the distinct carboxylic acids in the cyclic hydrogen bonded dimers in 2D and carboxylates in related 3D coordination polymers are discussed. All imaging was conducted in an alkanoic acid solvent to solubilize these polar polycarboxylates. The role of solvent cannot be neglected in the assembly patterns, and this point is addressed below in the broader context.

Results and Discussion

The molecular design strategy employed in this study involves the asymmetrical addition of a phenylene spacer between the central benzene ring and one or more carboxylic acids of **TMA** or isophthalic acid. Isophthalic acid (1,3-benzenedicarboxylic acid, **ISA**) is a reduced symmetry analogue of **TMA**, due to the decrease in number of carboxylic acids from three to two. The first two asymmetrical variations in the structure of **TMA** are made by the addition of phenylene spacers in one direction, thus reducing the point group symmetry from $\sim D_{3h}$ to $\sim C_{2v}$. The assigned point group symmetries throughout this work treat carboxylic acids as carboxylates to be consistent with the resolution achievable in the STM images. The biphenyl analogue of **TMA** (**1**) and the terphenyl analogue **2** (Figure 1) both have a 1:2 ratio of symmetry inequivalent carboxylic acids. If two phenylene rings are added between the central aromatic ring and two carboxylic acid moieties of **TMA**, then molecule **3** is obtained which, like **1**, **2**, and **ISA**, displays $\sim C_{2v}$ symmetry. Molecule **3** also has a 1:2 ratio of symmetry inequivalent carboxylic acids. The molecular symmetry of **ISA** is reduced to $\sim C_s$ by the insertion of a single phenylene ring between one car-

[a] Dr. R. A. Barnard, A. Dutta, Dr. J. K. Schnobrich, C. N. Morrison, Dr. S. Ahn, Prof. Dr. A. J. Matzger
Department of Chemistry and Macromolecular Science and Engineering
University of Michigan, 930 N. University Dr, Ann Arbor, MI 48109 (USA)
E-mail: matzger@umich.edu

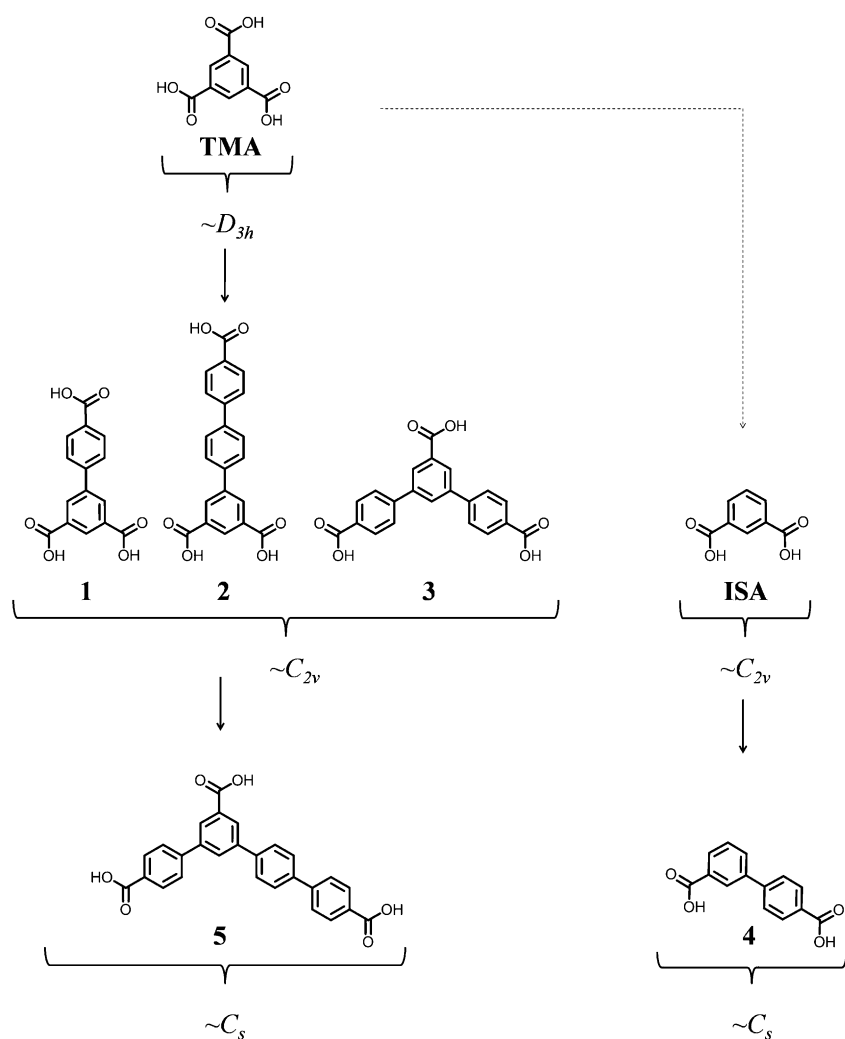Supporting information for this article is available on the WWW under http://dx.doi.org/10.1002/chem.201406332.

Figure 1. Molecular structures for the molecules investigated in this study. The dashed line represents a reduction in symmetry within the series by varying the number of carboxylic acid groups. The assigned point group symmetries treat carboxylic acids as carboxylates to be consistent with the resolution achievable in the STM images.

boxylic acid and the core benzene ring (**4**). Molecule **4** has a 1:1 ratio of symmetry inequivalent carboxylic acids. If a second phenylene spacer is added to molecule **3** between the central *meta*-substituted benzoic acid and one of the *para*-substituted benzoic acids, molecule **5** is derived. Molecule **5** has ~C_s symmetry and a 1:1:1 ratio of symmetry inequivalent carboxylic acids. Using STM, the pattern of the self-assembled monolayer(s) that each molecule forms at the solution/HOPG interface was examined. The relationship between the point group of each molecule with respect to the symmetry of the assembled network(s) will be discussed for each phase. In some cases more than one phase was observed and therefore each is discussed separately.

The 2D crystals of **TMA** and **ISA** have been investigated in the literature at solution/HOPG interfaces. Computed models of the known phases for each molecule are shown in Figure 2. The "chicken wire" phase of **TMA** is a planar array of fused hexagons with a **TMA** molecule at each vertex. The hexagonal pores are ~1 nm in diameter and have been shown to accommodate guest molecules.[4] The chicken wire phase incorpo-

rates only hydrogen-bonded dimers of **TMA**. The flower phase resembles the chicken wire phase in that it has hexagonal pores with a **TMA** molecule at each vertex, but in the flower phase these hexagons are not fused together. Instead, they are slightly offset such that a hydrogen bond trimer is formed at each of the corners of the hexagon with **TMA** molecules from two other hexagon vertices. This hydrogen bonded trimer forms a threefold axis of rotation. A small pore is present between the edges of adjacent hexagons in the flower phase. Both the chicken wire and flower phases are in the *p*6 plane group. A threefold axis of rotation lies on each **TMA** molecule in the chicken wire phase. However, in the flower phase, the threefold axis of rotation lies on the hydrogen-bonded trimer, not on the **TMA** molecules themselves. A close packing phase of **TMA** has been demonstrated in dilute, solvophobic conditions.[12] This phase forms with zig–zag lines of **TMA** molecules held together by hydrogen bonds between one carboxylic acid and the side of the dimers forming the zig–zag lines. This close packing phase is in the *p*2 plane group. Due to

the unique hydrogen bonding motif in the close packing phase, there are no threefold axes of rotation in that phase. **ISA** has one known phase: close packed ribbons of dimerized **ISA** molecules.[5] This 2D crystal is in the *p*2*gg* plane group. Structural features in the 2D crystals of the reduced symmetry analytes **1**–**5** from solution in *n*-heptanoic acid will be discussed in the context of the known phases of **TMA** and **ISA**.

Molecule 1 Phase I

Molecule **1** forms a phase consisting of columns of hydrogen bonded *meta*–*meta* dimers, shown in Figure 3. Due to the twofold symmetry from the hydrogen bonding of *meta*–*meta* dimers the apparent symmetry of this monolayer is *p*2. Plane group *p*2 is chiral, and the other enantiomer of this crystal is observed in separate domains; one such example is shown in Figure 3 c. Only homo-dimers are observed in the crystal. In other words, no cyclic hydrogen bonds are formed between *meta*- and *para*-substituted carboxylic acid moieties in this phase. The columns formed by dimers of **1** are separated by
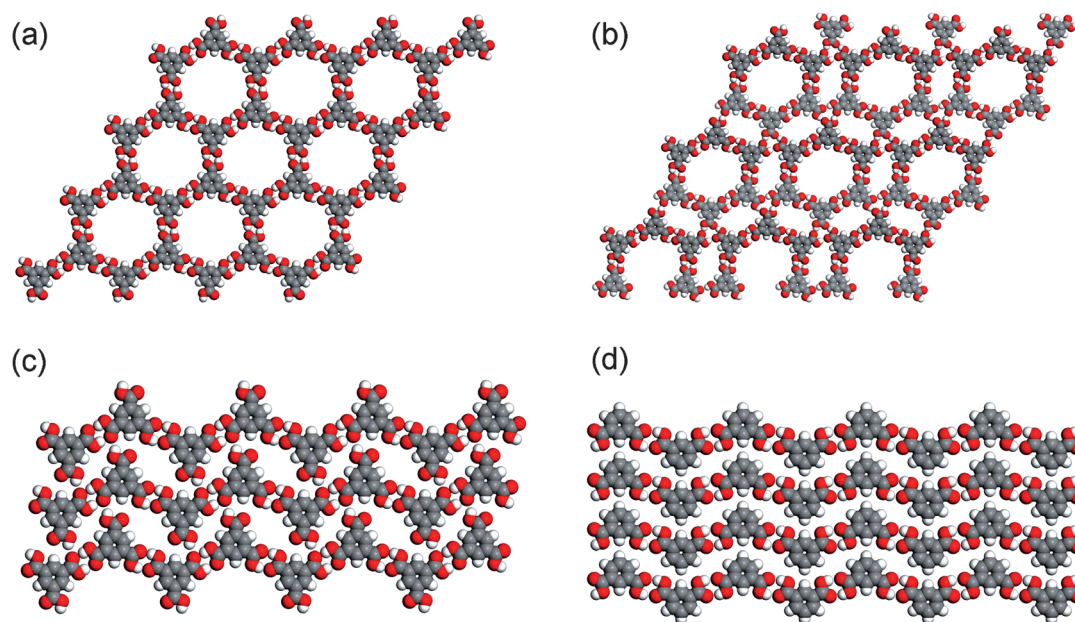
Figure 2. Computed models of a) the chicken wire phase of **TMA**,[2b,c] b) the flower phase of **TMA**,[2b,c] c) the close packing phase of **TMA**,[2j] and d) **ISA** 2D crystals[6b] based on literature STM studies at the solution/HOPG interface.
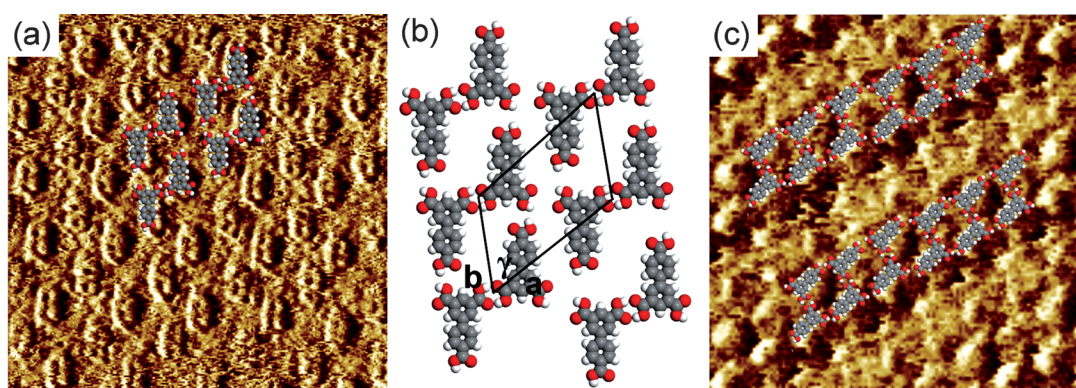

Figure 3. a) STM image (10×10 nm²) of Phase I formed by molecule **1** in *n*-heptanoic acid with overlaid molecular model, b) computed model of the crystal structure of Phase I of **1**, and c) STM image (10×10 nm²) of Phase I of molecule **1** formed in *n*-nonanoic acid.

5.79±0.47 Å, a space too wide to allow for even weak hydrogen bonding between the columns. Using nonanoic acid as the solvent, a longer chain alkyl fatty acid solvent than heptanoic acid, the space between the columns of dimers increases (Figure 3c) giving rise to a more apparent disordered region between these columns and supporting the notion that solvent inclusion exists between columns of **1** dimers.[6]

Molecule 1 Phase II

Molecule **1** forms a zig–zag phase, shown in Figure 4, of repeating *para–para* and *meta–meta* hydrogen-bonding dimers. The "dangling" *meta*-substituted carboxylic acid is assumed to interact with the protic solvent in the space between the zig–zag rows, similar to Phase I, and consistent with solvent incorporation. The length of the ribbon along the *meta–meta* dimer versus the *para–para* dimer results in an uneven herringbone-

type pattern (Figure 4c). This 2D crystal has the apparent symmetry of *p*2, with the twofold rotation axes at the center of each carboxylic acid homo-dimer. This phase is reminiscent of the ribbon phase of **ISA** (Figure 2d) but in this case the ribbons are slightly offset ($\gamma = 83.5 \pm 4.27°$) and the length of interacting units along the ribbon axis differ.

While both Phase I and II of molecule **1** incorporate only homo dimers, Phase I is built from *meta–meta* dimers and Phase II ribbons are composed of both *meta–meta* and *para–para* homodimers. Both phases are in the plane group *p*2, but in Phase I four of the nine twofold rotation axes lie on the homo-dimers and six of the nine twofold rotation axes lie on the homo-dimers in Phase II. While the motifs differ in local arrangement, columns of dimers (Phase I) versus ribbons (Phase II), both phases incorporate only one unique molecule ($Z' = 1$).

The carboxylate analogue of biphenyl tritopic linker **1** has been used to direct microporous coordination polymer (MCP)
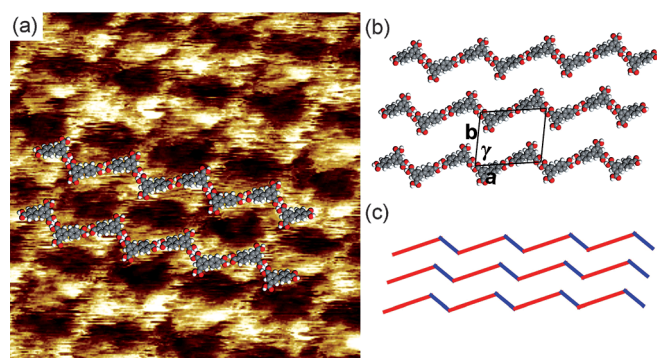
Figure 4. a) STM images (10×10 nm²) of Phase II of **1** formed in heptanoic acid, b) computed model of the crystal structure of zig-zag pattern, and c) cartoon of the zig-zag phase highlighting the distorted herringbone pattern.

architecture.[7] It is the organic linker in the material UMCM-150,[8] the first material used to demonstrate reduced symmetry linkers as a route to preventing interpenetration in crystalline porous materials.[3] In UMCM-150, the two symmetry inequivalent carboxylates segregate at the metal nodes: the isophthalate carboxylates form copper paddlewheels and the *para*-benzoates form the unusual copper cluster $Cu_3(O_2CR)_6$ (see the Supporting Information). The 1:2 ratio of symmetry inequivalent carboxylates requires more than one type of copper cluster to be present in a given structure.[3] In contrast, **TMA** has only symmetry equivalent carboxylate and HKUST-1, the MCP which incorporates the carboxylate version of **TMA** as the organic linker, has only one kind of copper cluster (see the Supporting Information).[9] The consequence of the statistical requirement in UMCM-150 is that there are two kinds of copper clusters and the carboxylates segregate between them within the structure.[3] In 2D assembly, and without the presence of a metal center, if all carboxylic acids are dimerized it is not possible to have a single mode of association for **1** because of the stoichiometric imbalance of *para* and *meta* substitutions. In fact, carboxylic acid segregation is present in the monolayers and all **1**–**1** interactions are homo dimers: *meta*–*meta* or *para*–*para*.

Molecule 2

The *para*-terphenyl derived tritopic linker, **2**, forms a phase with small pores as shown in Figure 5. The motif is formed by chains of repeating *meta*–*meta* dimers where the *para*-substituted carboxylic acids point in alternating directions along the *b* axis of the crystal. The *para*-substituted carboxylic acids form homo-dimers linking the chains of *meta*–*meta* dimers and completing the elongated hexagonal pores (2.85×1.24 nm²). This porous phase is an extended version of the chicken wire phase of **TMA** (Figure 2 a). According to the molecular design strategy, molecule **2** is obtained when two phenylene rings are added between the central benzene ring and the same carboxylic acid of **TMA** (Figure 1). The added phenylene rings align with the *b* axis in the crystal thus distorting the hexagonal chicken wire pores. With the loss of the threefold symmetry as

compared to **TMA**, the monolayer also loses threefold symmetry features and lies in the rectangular plane group *cm*. Molecule **2** has not been shown to form a MCP, and as such no comparisons can be drawn between 2D monolayer and 3D behavior.
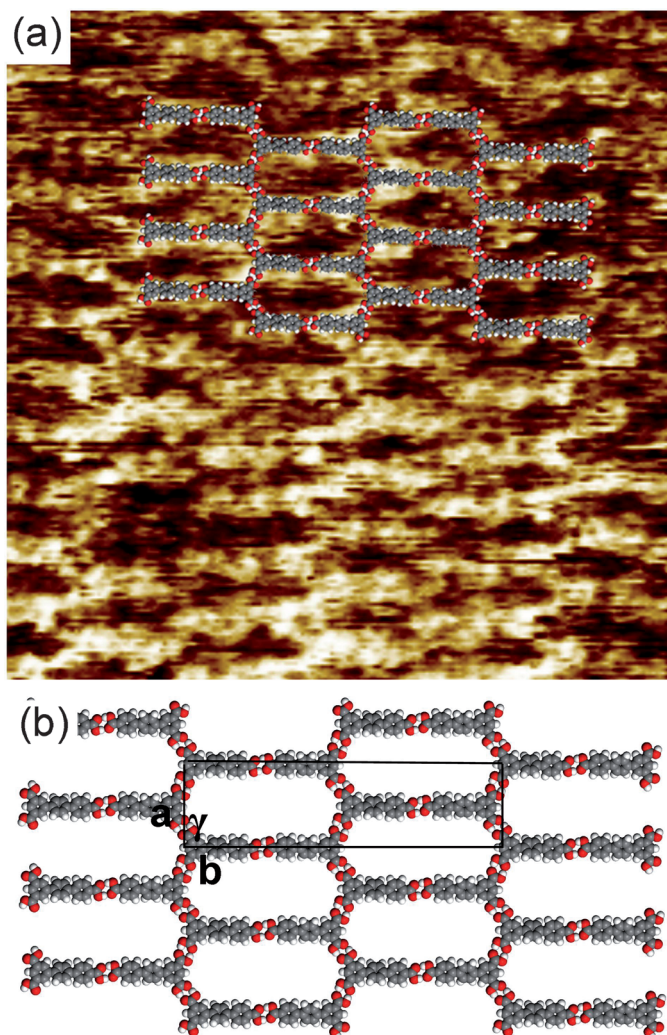

Figure 5. a) STM image (20×20 nm²) of the monolayer **2** with overlaid model and b) the computed model of 2D crystal structure of **2**.

Molecule 3

The *meta*-terphenyl tritopic linker, **3**, forms a ribbon phase, shown in Figure 6. The **3**–**3** hydrogen-bond dimers are composed of *trans-meta*–*meta* cyclic dimers (Figure 6 b). This phase is similar to that of **ISA** (Figure 2 d) in that both have a 120° angle between the *trans*-homo-dimers along a given ribbon, meaning that the other *para*-substituted carboxylic acids lie on opposite sides of the plane that contains the cyclic hydrogen-bond dimer. Unlike Phase II of molecule **1**, interacting units along the ribbon axis for each homo-dimer are of equal length. The apparent symmetry of this 2D crystal is *p2mg*, a very uncommon plane group according to the 2D Structural Database;[1a] there are only two other compounds in the database that have monolayers with *p2mg* symmetry.[10]
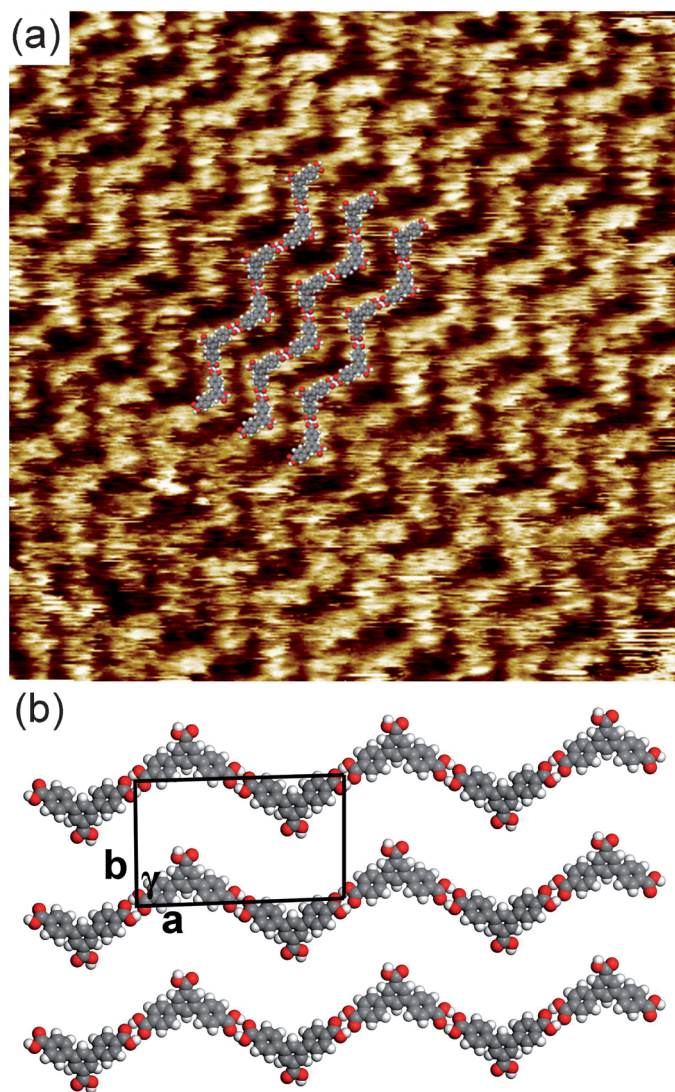
cules ($Z' = 2$) and as such is the only ordered phase in the series to incorporate more than one building block.

The carboxylate version of molecule **4** has been used as the organic linker in two isomeric MCPs.[11] Both isomers are comprised of copper paddlewheels of two *meta*- and two *para*-carboxylates and vary in the coordination modes of the carboxylates at the paddlewheels. In one structure the carboxylate substitutions alternate around the Cu–Cu axis in a *meta–para–meta–para* arrangement. In the other isomer the sequence of carboxylate substitution around the Cu-Cu axis is *meta–meta–para–para* (see the Supporting Information). The lack of carboxylate segregation is possible due to the 1:1 ratio of symmetry inequivalent carboxylates in **4**. More than one kind of paddlewheel is not required in a given structure to satisfy the stoichiometry of the carboxylates. The 1:1 ratio of symmetry inequivalent moieties in **4** results in mixed copper paddlewheels in 3D and hetero-dimers in 2D.

Molecule 5

Tritopic quaterphenyl linker **5** has three symmetry inequivalent carboxylic acids. The primary monolayer motif formed by **5** has no regular, repeating pattern (Figure 8). In contrast to the examples of large scale disorder[12] in the Two-Dimensional Structural Database (2DSD),[1a] this assembly does not show areas of local order. Thermal annealing, dilution, and solvophobic conditions have been used in pursuit of obtaining an ordered phase for **5** and have thus far been unsuccessful.

The three carboxylic acids are symmetry inequivalent, resulting in at least 12 unique dimers that could be formed by molecule **5** in 2D. The availability of so many competing arrangements may contribute to the formation of the disorder[13] at the solution/HOPG interface. Molecule **5** has not been shown to form a MCP, and as such no comparisons can be drawn between 2D monolayer and 3D behavior.

The monolayers formed from the five reduced symmetry analogues of **TMA** and **ISA** examined in this study show a strong dependence on the symmetry of the hydrogen-bonded dimer in determining the structure of the resulting 2D crystals. Table 1 summarizes the point group for the deprotonated structure of each molecule and the plane group for each monolayer based on the apparent symmetry in the image. The threefold axis of rotation in the apparent symmetry in monolayers of **TMA** was lost in monolayers assembled from molecules in this design strategy. Only one monolayer in this series does not incorporate homomeric hydrogen bonding (**4**) and that monolayer lies in the plane group *p*1. Of the five ordered monolayers formed from this series, four different plane groups were observed. In contrast, the 2D crystals formed from reduced symmetry analogues of 1,3,5-benzenetribenzoic acid (H$_3$BTB) all exhibited *p*2 symmetry.[14] From a molecular design perspective, **TMA** and **ISA** are the higher symmetry molecules that were used as the starting points for this route to a series of reduced symmetry multicarboxylated arenes through the addition of phenylene spacers (Figure 1). Both **TMA** and **ISA** have only symmetry equivalent carboxyl groups.

Figure 6. a) STM image (25×25 nm^2) of the monolayer **3** with overlaid model and b) the computed model of 2D crystal structure of **3**.

The carboxylate form of molecule **3** has been incorporated into the MCP UMCM-151, where the symmetry inequivalent carboxylates segregate such that each copper paddlewheel is coordinated by only *para*- or *meta*-substituted carboxylates (see the Supporting Information).[3] To satisfy stoichiometry, there are two times as many *para*-coordinated paddlewheels as there are *meta*-coordinated paddlewheels. Similar to molecule **1**, in the case of **3** the 1:2 ratio of symmetry inequivalent carboxylates requires more than one kind of paddlewheel coordination in the MCP structure.

Molecule 4

The phase formed by molecule **4** is a ribbon structure exclusively incorporating hetero dimers (Figure 7). With the *meta–para* hydrogen bonds, the lack of twofold rotation axes, and an offset alignment of neighboring ribbons the 2D crystal is in the plane group *p*1. This motif is built from two unique mole-
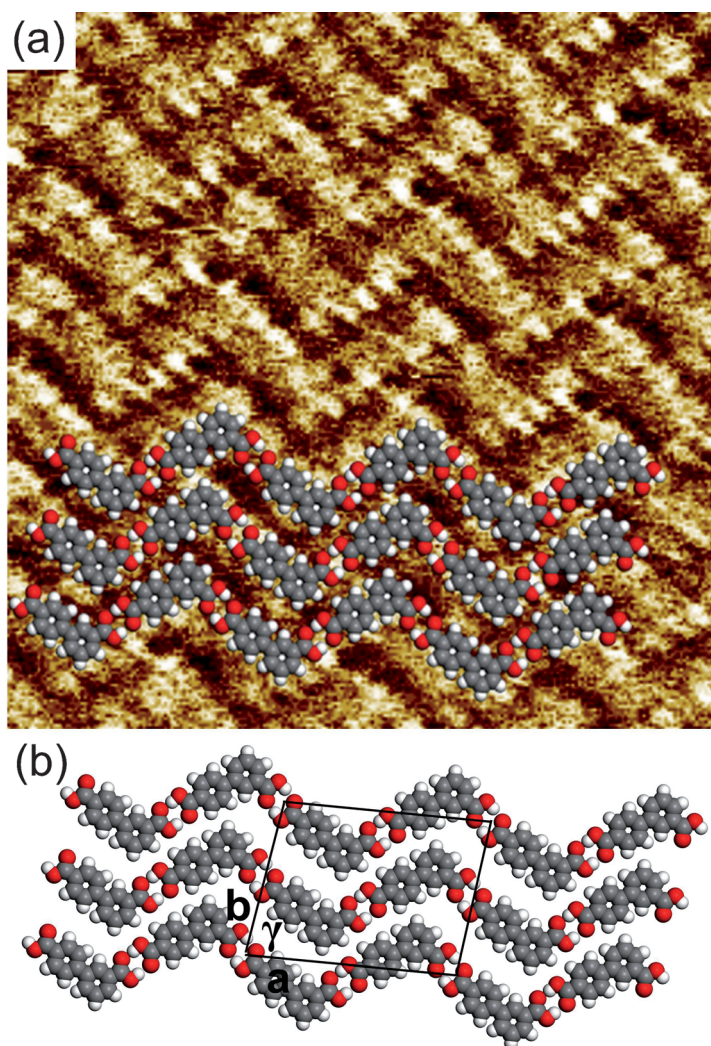
Figure 7. a) STM image (10×10 nm²) of the monolayer of **4** with overlaid model and b) the computed model of 2D crystal structure of **4**.
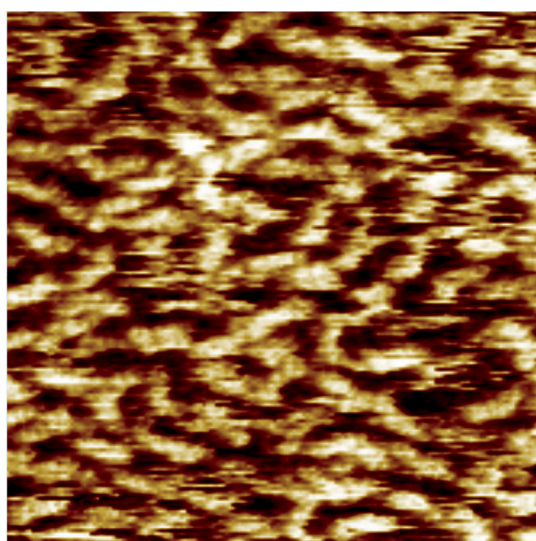

Figure 8. STM image (25×25 nm²) of the monolayer of molecule **5** exhibiting disorder.

For this series (Table 1), where there are only homo-dimers in 2D (molecules 1, 2, and 3), any symmetry inequivalent carboxylates are phase segregated in the 3D MCPs such that only one kind of carboxylate symmetry is present at each metal cluster. In the case of 4, where hetero-dimers are formed in 2D, the metal centers in the MCP have a mixture of substituted carboxylates. There are no monolayers in this series with mixed hetero- and homo-dimers. In contrast, for a tetracarboxylate derivative of H₃BTB (5'-(4-carboxyphenyl)-[1,1':3',1''-terphenyl]-3,4'',5-tricarboxylic acid), both homo- and hetero-dimers are formed in 2D[14] and the substitution of the carboxylates at each metal center in the two MPCs are mixed.[3] This is, perhaps, not surprising in light of different geometry requirements to fill space in 2D and 3D.

Conclusion

We have designed a series of five molecules related to **TMA**, an archetypal high symmetry adsorbate, through the addition of phenylene spacers. In contrast to monolayers formed from alternate routes to reduced symmetry adsorbates, self-assembly of molecules in this series yields six monolayers in five different plane groups. The composition of the cyclic carboxylic acid dimers (homo- or hetero-dimers) in the resultant 2D crystals at the liquid/HOPG interface is related to the stoichiometric ratio of symmetry inequivalent carboxylic acids of each analyte, and solvent inclusion is important for stabilizing carboxylic acids in the majority of the structures observed. Additionally, the analyte with a 1:1:1 ratio of symmetry inequivalent carboxylic acids (**5**) formed a disorderd phase at the solution/HOPG interface. The composition of the dimers in 2D (homo or hetero) mirrors the carboxylates composition (*meta*- or *para*-substituted) at the metal centers in MCPs incorporating these carboxylated arenes as the organic linkers. Such findings have design implications for using molecular symmetry to guide complex assemblies in both 2D and 3D.

Table 1. Summary of relevant crystallographic information pertaining to the molecules of interest and the two-dimensional crystals formed.

Name	Point group[a]	Hydrogen-bonding interaction	Plane group	Z'
TMA	~D_{3h}	homo-dimer	$p6$	1/3
		homo- & hetero-dimer	$p6$	1
		homo-dimer & side	$p2$	1
1	~C_{2v}	homo-dimer	$p2$	1
		homo-dimer	$p2$	1
2	~C_{2v}	homo-dimer	cm	1
3	~C_{2v}	homo-dimer	$p2mg$	1/2
ISA	~C_{2v}	homo-dimer	$p2gg$	1/2
4	~C_s	hetero-dimer	$p1$	4
5	~C_s	disorder	n/a	n/a

[a] Point groups are assigned for deprotonated structures.

Experimental Section

Materials: Compounds **1**,[15] **3**,[8] and **4**[11] were synthesized according to literature methods. Heptanoic acid (98%) was purchased from Acros Organics. The syntheses for **2** and **5** are described below.

3,4″,5-Trimethyl-*para*-terphenyl: 4-Bromo-4′-methylbiphenyl (1.56 g, 10.4 mmol), 3,5-dimethylphenylboronic acid (2.00 g, 9.43 mmol), toluene (40 mL), EtOH (30 mL), and 2 M aqueous Na$_2$CO$_3$ (30 mL) were added into a pressure vessel equipped with a magnetic stir bar. The resulting mixture was sparged with N$_2$ gas for 15 min. Pd(PPh$_3$)$_4$ was added into the mixture, vessel was sealed, and the mixture was heated at 85 °C for 18 h. After cooling the reaction mixture to room temperature diethyl ether (200 mL) was added to the mixture. The organic and aqueous layers were separated, and the aqueous layer was extracted with diethyl ether (3×100 mL). The organic layers were combined and dried over anhydrous Na$_2$SO$_4$. The organic layer was filtered and the solvent was removed under reduced pressure. The residue was recrystallized from a mixture of CH$_2$Cl$_2$/hexane at 0 °C to produce a white solid (1.73 g, yield 67.4%). ^{1}H NMR (500 MHz, CDCl$_3$): δ = 7.64 (s, 4H), 7.56 (d, 2H, J = 7.9 Hz), 7.28–7.26 (m, 4H), 7.01 (s, 1H), 2.41 (s, 3H), 2.39 (s, 6H); ^{13}C NMR (125 MHz, CDCl$_3$): δ = 140.93, 140.22, 140.00, 138.44, 138.04, 137.21, 129.67, 129.07, 127.63, 127.32, 127.02, 125.12, 21.58, 21.28.

***para*-Terphenyl-3,4″,5-tricarboxylic acid (2)**: 3,4″,5-Trimethyl-*para*-terphenyl (0.5 g, 1.8 mmol), KMnO$_4$ (0.87 g, 5.5 mmol), H$_2$O (20 mL), and pyridine (20 mL) were added in a round bottom flask equipped with a magnetic stir bar and the mixture was heated to reflux for 3 d. Additional aliquots of KMnO$_4$ (8×0.87 g, 5.5 mmol) were added during this period. After cooling the reaction mixture to room temperature the mixture was filtered over a plug of celite. The filtrate was evaporated and the residue was dissolved in water (100 mL). Insoluble solid was filtered off and the filtrate was acidified with concentrated HCl. The white precipitate was collected by filtration, washed thoroughly with H$_2$O, and dried under vacuum to afford **2** (0.75 g, yield 64.6%). ^{1}H NMR (500 MHz, [D$_6$]DMSO): δ = 13.39 (br s, 3H), 8.49 (s, 1H), 8.42 (s, 2H), 8.05 (d, 2H, J = 8.3 Hz), 7.92–7.85 (m, 6H); ^{13}C NMR (125 MHz, [D$_6$]DMSO): δ = 167.18, 166.78, 143.39, 139.97, 138.67, 138.46, 130.75, 130.10, 130.03, 129.08, 127.75, 127.55, 127.41, 126.74; HRMS (EI): m/z: calcd for C$_{21}$H$_{14}$O$_6$: 362.0790; found: 362.0791.

Methyl 4′-pinacolatoboronbiphenyl-4-carboxylate: Methyl 4′-bromobiphenyl-4-carboxylate (2.50 g, 8.61 mmol), [bis-pinacolato]diboron (2.62 g, 10.32 mmol), KOAc (2.50 g, 25.8 mmol), and 1,4-dioxane (150 mL) were added to a pressure vessel equipped with a magnetic stir bar. The resulting mixture was sparged for 1 h with N$_2$ gas. Pd(dppf)Cl$_2$ (0.21 g, 0.43 mmol) was added into the mixture, vessel was sealed, and the mixture was heated to reflux for 48 h. After cooling the reaction mixture to room temperature the solvent was removed under reduced pressure. The residue was dissolved in CH$_2$Cl$_2$ (150 mL) and washed with H$_2$O (3×100 mL) followed by brine (200 mL). The organic layer was dried over anhydrous MgSO$_4$, filtered, and the solvent was removed under reduced pressure. The crude product was subjected to gradient column chromatography (hexanes/ethyl acetate) to yield pure white solid (2.18 g, yield 73.1%). ^{1}H NMR (500 MHz, CDCl$_3$): δ = 8.12 (d, 2H, J = 8.3 Hz), 7.90 (d, 2H, J = 8.2 Hz), 7.68 (d, 2H, J = 8.3 Hz), 7.64 (d, 2H, J = 8.2 Hz), 3.94 (s, 3H), 1.37 (s, 12H); ^{13}C NMR (125 MHz, CDCl$_3$): δ = 167.12, 145.58, 142.73, 135.51, 130.23, 129.28, 127.30, 126.71, 84.08, 52.30, 25.03.

Dimethyl 5-bromobiphenyl-3,4′-dicarboxylate: Methyl 3,5-dibromobenzoate (15.0 g, 51.0 mmol), 4-(methoxycarbonyl)phenylboronic acid (6.12 g, 34.0 mmol), K$_2$CO$_3$ (5.63 g, 40.8 mmol), 200 mL 1,4-dioxane, and 20 mL H$_2$O were added in a pressure vessel equipped with a magnetic stir bar. The resulting mixture was sparged for 1 h with N$_2$ gas. Pd(PPh$_3$)$_4$ (2.01 g, 3.41 mmol) was added into the sparged mixture, vessel was sealed, and the mixture was heated to reflux for 48 h. After cooling the reaction mixture to room temperature the solvent was removed under reduced pressure. The residue was dissolved in CH$_2$Cl$_2$ (200 mL) and washed with H$_2$O (3× 200 mL) followed by brine (300 mL). The organic layer was dried over anhydrous MgSO$_4$, filtered, and the solvent was removed under reduced pressure. The crude product was subjected to gradient column chromatography (hexanes/ethyl acetate) to yield pure white solid (6.51 g, yield 54.8%). ^{1}H NMR (500 MHz, CDCl$_3$): δ = 8.22 (t, 1H, J = 1.6 Hz), 8.19 (t, 1H, J = 1.7 Hz), 8.16–8.11 (m, 2H), 7.94 (t, 1H, J = 1.84 Hz), 7.69–7.64 (m, 2H), 3.96 (s, 3H), 3.95 (s, 3H); ^{13}C NMR (125 MHz, CDCl$_3$): δ = 166.83, 165.70, 143.13, 142.38, 134.57, 134.68, 132.09, 130.47, 130.11, 127.28, 127.22, 123.20, 52.75, 52.42.

[1,1′:3′,1″:4″,1‴-Quaterphenyl]-4,4‴,5′-tricarboxylic acid (5): Methyl 4′-pinacolatoboronbiphenyl-4-carboxylate (1.50 g, 4.44 mmol), dimethyl 5-bromo-biphenyl-3,4′-dicarboxylate (1.40 g, 4.04 mmol), K$_2$CO$_3$ (1.95 g, 14.1 mmol), THF (70 mL), and H$_2$O (10 mL) were added in a pressure vessel equipped with a magnetic stir bar. The resulting mixture was sparged for 1 h with N$_2$ gas. Pd(PPh$_3$)$_4$ (0.465 g, 0.403 mmol) was added to the mixture, vessel was sealed, and the mixture was heated to reflux for 48 h. After cooling the reaction mixture to room temperature the solvent was removed under reduced pressure. The residue was dissolved in CH$_2$Cl$_2$ (150 mL) and washed with H$_2$O (3×100 mL) followed by brine (200 mL). The organic layer was dried over anhydrous MgSO$_4$, filtered, and the solvent was removed under reduced pressure. The crude product was subjected to gradient column chromatography (hexanes/ethyl acetate) to yield pure white solid. This white solid (1.31 g, 2.73 mmol), 1,4-dioxane (40 mL), H$_2$O (40 mL), and KOH (1.53 g, 27.3 mmol) were added into a pressure vessel equipped with a magnetic stir bar. The resultant suspension was heated to reflux for 12 h. After cooling to room temperature the reaction mixture was filtered and the solvent was removed under reduced pressure. The residue was dissolved in H$_2$O (200 mL) and the solution was acidified with concentrated HCl until the pH of the solution was 2. The target compound was collected by filtration, washed thoroughly with H$_2$O, and dried under vacuum to afford **5** (1.01 g, yield 90.9%). ^{1}H NMR (700 MHz, [D$_6$]DMSO): δ = 13.10 (br s, 3H), 8.26–8.20 (m, 2H), 8.10–8.04 (m, 4H), 7.96–7.88 (m, 4H), 7.86–7.80 (m, 4H); ^{13}C NMR (175 MHz, [D$_6$]DMSO): δ = 167.20, 167.17, 167.07, 143.63, 143.32, 140.78, 140.34, 138.85, 138.64, 132.52, 130.25, 130.12, 130.08, 129.84, 129.52, 127.77, 127.64, 127.41, 127.30, 127.05, 126.86, 126.79; HRMS (EI): m/z: calcd for C$_{27}$H$_{18}$O$_6$: 438.1103; found: 438.1099.

Scanning tunneling microscopy: A Nanoscope E STM (Digital Instruments) was used for all imaging. Highly oriented pyrolytic graphite (HOPG) (SPI-1 grade, Structure Probe Inc.) was used as a substrate for monolayer formation. A heptanoic acid solution of the desired molecule was made, of which 2 μL was placed on freshly cleaved HOPG to obtain a self-assembled monolayer. Each solution was at or near saturation in heptanoic acid. STM tips were made from Pt/Ir (20% Ir, 0.010 inch diameter, California Fine Wire) by mechanical cutting. Imaging was performed under ambient conditions and typical STM settings consist of 300 pA current and 700–900 mV bias voltage (sample positive). All images are unfiltered. For a specific image, the cell constants may vary from the average due to the drift of the STM tip. Cell constants and symme-

tries were determined by examining several images of both scan directions to account for this phenomenon.

Computational modeling: Molecular mechanics modeling of the 2D assemblies was performed in Materials Studio version 4.3 (Accelrys Software Inc.) using the assembled patterns and symmetry resolved in STM images with solvent omitted. Each lattice was geometry optimized in the Forcite module using the COMPASS force field[16] without molecule or lattice constraints. This method has been shown to correctly describe the geometry and relative energy stability of 3D polymorphic arrangements in molecular crystals.[17] Models of each lattice were built such that a layer of the model in the *ab* plane represents the arrangement of molecules observed in the STM images for a given phase. The *c* axis, which is the distance between monolayers, was set to 100 Å for all models to minimize intermolecular interactions out of the *ab* plane and this axis changed less than 3 Å during optimization.

Acknowledgements

[1] a) K. E. Plass, A. L. Grzesiak, A. J. Matzger, *Acc. Chem. Res.* **2007**, *40*, 287–293; b) A. I. Kitaigorodskii, *Organic Chemical Crystallography*, Consultants Bureau, New York, **1959**.

[2] a) L. Kampschulte, M. Lackinger, A.-K. Maier, R. S. K. Kishore, S. Griessl, M. Schmittel, W. M. Heckl, *J. Phys. Chem. B* **2006**, *110*, 10829–10836; b) M. Lackinger, S. Griessl, W. M. Heckl, M. Hietschold, G. W. Flynn, *Langmuir* **2005**, *21*, 4984–4988; c) S. Griessl, M. Lackinger, M. Edelwirth, M. Hietschold, W. M. Heckl, *Single Mol.* **2002**, *3*, 25–31; d) M. Lackinger, S. Griessl, L. Kampschulte, F. Jamitzky, W. M. Heckl, *Small* **2005**, *1*, 532–539; e) H. Zhou, H. Dang, J.-H. Yi, A. Nanci, A. Rochefort, J. D. Wuest, *J. Am. Chem. Soc.* **2007**, *129*, 13774–13775; f) L. Kampschulte, T. L. Werblowsky, R. S. K. Kishore, M. Schmittel, W. M. Heckl, M. Lackinger, *J. Am. Chem. Soc.* **2008**, *130*, 8502–8507; g) G.-J. Su, H.-M. Zhang, L.-J. Wan, C.-L. Bai, T. Wandlowski, *J. Phys. Chem. B* **2004**, *108*, 1931–1937; h) Z. Li, B. Han, L. J. Wan, T. Wandlowski, *Langmuir* **2005**, *21*, 6915–6928; i) J. M. MacLeod, O. Ivasenko, C. Fu, T. Taerum, F. Rosei, D. F. Perepichka, *J. Am. Chem. Soc.* **2009**, *131*, 16844–16850; j) N. T. N. Ha, T. G. Gopakumar, R. Gutzler, M. Lackinger, H. Tang, M. Hietschold, *J. Phys. Chem. C* **2010**, *114*, 3531–3536.

[3] J. K. Schnobrich, O. Lebel, K. A. Cychosz, A. Dailly, A. G. Wong-Foy, A. J. Matzger, *J. Am. Chem. Soc.* **2010**, *132*, 13941–13948.

[4] a) S. J. H. Griessl, M. Lackinger, F. Jamitzky, T. Markert, M. Hietschold, W. M. Heckl, *Langmuir* **2004**, *20*, 9403–9407; b) J. Liu, X. Zhang, H.-J. Yan, D. Wang, J.-Y. Wang, J. Pei, L.-J. Wan, *Langmuir* **2010**, *26*, 8195–8200; c) S. J. H. Griessl, M. Lackinger, F. Jamitzky, T. Markert, M. Hietschold, W. M. Heckl, *J. Phys. Chem. B* **2004**, *108*, 11556–11560.

[5] M. Lackinger, S. Griessl, T. Markert, F. Jamitzky, W. M. Heckl, *J. Phys. Chem. B* **2004**, *108*, 13652–13655.

[6] a) F. Tao, J. Goswami, S. L. Bernasek, *J. Phys. Chem. B* **2006**, *110*, 19562–19569; b) K. G. Nath, O. Ivasenko, J. M. MacLeod, J. A. Miwa, J. D. Wuest, A. Nanci, D. F. Perepichka, F. Rosei, *J. Phys. Chem. C* **2007**, *111*, 16996–17007.

[7] a) Z.-J. Lin, B. Xu, T.-F. Liu, M.-N. Cao, J. Lü, R. Cao, *Eur. J. Inorg. Chem.* **2010**, *2010*, 3842–3849; b) C.-S. Lim, J. K. Schnobrich, A. G. Wong-Foy, A. J. Matzger, *Inorg. Chem.* **2010**, *49*, 5271–5275; c) C.-C. Ji, J. Li, Y.-Z. Li, Z.-J. Guo, H.-G. Zheng, *CrystEngComm* **2011**, *13*, 459; d) L. Li, S. Wang, T. Chen, Z. Sun, J. Luo, M. Hong, *Cryst. Growth Des.* **2012**, *12*, 4109–4115; e) Y. Lu, W. Zhao, Y. Liu, B. Liu, X. Feng, J. Tan, X. Li, X. Yang, *J. Solid State Chem.* **2012**, *192*, 144–152; f) Z. Guo, H. Xu, S. Su, J. Cai, S. Dang, S. Xiang, G. Qian, H. Zhang, M. O'Keeffe, B. Chen, *Chem. Commun.* **2011**, *47*, 5551; g) Z. Zhang, L. Zhang, L. Wojtas, P. Nugent, M. Eddaoudi, M. J. Zaworotko, *J. Am. Chem. Soc.* **2012**, *134*, 924–927; h) W.-W. He, S.-L. Li, W.-L. Li, J.-S. Li, G.-S. Yang, S.-R. Zhang, Y.-Q. Lan, P. Shen, Z.-M. Su, *J. Mater. Chem. A* **2013**, *1*, 11111–11116; i) T. Liu, S. Wang, J. Lu, J. Dou, M. Niu, D. Li, J. Bai, *CrystEngComm* **2013**, *15*, 5476–5489; j) L. Li, S. Zhang, L. Han, Z. Sun, J. Luo, M. Hong, *Cryst. Growth Des.* **2013**, *13*, 106–110.

[8] A. G. Wong-Foy, O. Lebel, A. J. Matzger, *J. Am. Chem. Soc.* **2007**, *129*, 15740–15741.

[9] S. S.-Y. Chui, S. M.-F. Lo, J. P. H. Charmant, A. G. Orpen, I. D. Williams, *Science* **1999**, *283*, 1148–1150.

[10] a) K. E. Plass, K. Kim, A. J. Matzger, *J. Am. Chem. Soc.* **2004**, *126*, 9042–9053; b) J. P. Rabe, S. Buchholz, L. Askadskaya, *Synth. Met.* **1993**, *54*, 339–349; c) C. L. Claypool, F. Faglioni, W. A. Goddard, H. B. Gray, N. S. Lewis, R. A. Marcus, *J. Phys. Chem. B* **1997**, *101*, 5978–5995.

[11] L. Feng, Z. Chen, T. Liao, P. Li, Y. Jia, X. Liu, Y. Yang, Y. Zhou, *Cryst. Growth Des.* **2009**, *9*, 1505–1510.

[12] a) E. Mena-Osteritz, *Adv. Mater.* **2002**, *14*, 609–616; b) T. Kirschbaum, R. Azumi, E. Mena-Osteritz, P. Bauerle, *New J. Chem.* **1999**, *23*, 241–250; c) P. Samorì, X. Yin, N. Tchebotareva, Z. Wang, T. Pakula, F. Jäckel, M. D. Watson, A. Venturini, K. Müllen, J. P. Rabe, *J. Am. Chem. Soc.* **2004**, *126*, 3567–3575; d) M. Fischer, G. Lieser, A. Rapp, I. Schnell, W. Mamdouh, S. De Feyter, F. C. De Schryver, S. Höger, *J. Am. Chem. Soc.* **2003**, *125*, 214–222.

[13] S. L. Price, *Chem. Soc. Rev.* **2014**, *43*, 2098–2111.

[14] C. N. Morrison, S. Ahn, J. K. Schnobrich, A. J. Matzger, *Langmuir* **2011**, *27*, 936–942.

[15] J.-R. Li, H.-C. Zhou, *Angew. Chem. Int. Ed.* **2009**, *48*, 8465–8468; *Angew. Chem.* **2009**, *121*, 8617–8620.

[16] H. Sun, *J. Phys. Chem. B* **1998**, *102*, 7338–7364.

[17] K. R. Mitchell-Koch, A. J. Matzger, *J. Pharm. Sci.* **2008**, *97*, 2121–2129.